Monthly Notices
of the
ROYAL ASTRONOMICAL SOCIETY

MNRAS **454,** 3391–3402 (2015) doi:10.1093/mnras/stv2065

Radio haloes in Sunyaev–Zel'dovich-selected clusters of galaxies: the making of a halo?

A. Bonafede,[1⋆] H. Intema,[2] M. Brüggen,[1] F. Vazza,[1] K. Basu,[3] M. Sommer,[3] H. Ebeling,[4] F. de Gasperin,[1] H. J. A. Röttgering,[5] R. J. van Weeren[6] and R. Cassano[7]

[1]*Hamburger Sternwarte, Universität Hamburg, Gojenbergsweg 112, 21029 Hamburg, Germany*
[2]*National Radio Astronomy Observatory, 1003 Lopezville Road, Socorro, NM 87801-0387, USA*
[3]*Argelander Institut für Astronomie, Universität Bonn, D-53121 Bonn, Germany*
[4]*Institute for Astronomy, University of Hawaii, 2680 Woodlawn Drive, Honolulu, HI 96822, USA*
[5]*Leiden Observatory, Leiden University, PO Box 9513, 2300RA Leiden, the Netherlands*
[6]*Harvard-Smithsonian Center for Astrophysics, 60 Garden Street, Cambridge, MA 02138, USA*
[7]*INAF IRA, via Gobetti 101, 40129 Bologna, Italy*

Accepted 2015 September 2. Received 2015 September 2; in original form 2015 June 17

ABSTRACT

Radio haloes are synchrotron radio sources detected in some massive galaxy clusters. Their size of Mpc indicates that (re)acceleration processes are taking place in the host cluster. X-ray catalogues of galaxy clusters have been used in the past to search for radio haloes and to understand their connection with cluster–cluster mergers and with the thermal component of the intracluster medium. More recently, the Sunyaev–Zel'dovich effect has been proven to be a better route to search for massive clusters in a wider redshift range. With the aim of discovering new radio haloes and understanding their connection with cluster–cluster mergers, we have selected the most massive clusters from the *Planck* early source catalogue and we have observed with the Giant Metrewave Radio Telescope at 323 MHz those objects for which deep observations were not available. We have discovered new peculiar radio emission in three of the observed clusters, finding (i) a radio halo in the cluster RXCJ0949.8+1708, (ii) extended emission in Abell 1443 that we classify as a radio halo plus a radio relic, with a bright filament embedded in the radio halo, and (iii) low-power radio emission in CIZA J1938.3+5409 that is ten times below the radio–X-ray correlation and represents the first direct detection of the radio emission in the 'upper-limit' region of the radio–X-ray diagram. We discuss the properties of these new radio haloes in the framework of theoretical models for the radio emission.

Key words: acceleration of particles – radiation mechanisms: non-thermal – galaxies: clusters: individual: Abell 1443 – galaxies: clusters: individual: CIZAJ1938.3+5409 – galaxies: clusters: individual: RXCJ0949.9+1708 – galaxies: clusters: individual: RXCJ1354.6+7715.

1 INTRODUCTION

Some galaxy clusters host diffuse radio emission that is not directly connected to any of the cluster radio galaxies. This emission fills the inner Mpc of the host cluster (radio halo) or is located at the cluster periphery (radio relics) and is characterized by a low surface brightness at $\nu \sim 1.4$ GHz (~ 1 μJy arcsec^{-2}) and a steep radio spectrum[1] with $\alpha > 1$ (see e.g. the review by Feretti et al. 2012).

Radio haloes are produced by ultrarelativistic electrons, with Lorentz factors $\gamma_L \sim 10^4$, spinning in large-scale μG magnetic fields. The radio power at 1.4 GHz ($P_{1.4\,\mathrm{GHz}}$) correlates with the X-ray luminosity (L_X) of the host cluster (e.g. Liang et al. 2000). Since L_X is a proxy of the cluster mass, this correlation indicates that more massive systems host more powerful radio haloes. In addition, a radio bi-modality is found in the L_X–$P_{1.4\,\mathrm{GHz}}$ plane (Brunetti et al. 2009): clusters with the same X-ray luminosity either host a radio halo, the power of which follows the L_X–$P_{1.4\,\mathrm{GHz}}$ correlation (referred to as the 'radio-on state'), or do not host radio emission at all ('radio-off state').

From a statistical point of view, not only the power but also the occurrence of radio haloes is known to increase with L_X and hence with the mass of the host cluster (e.g. Giovannini, Tordi & Feretti 1999; Cuciti et al. 2015).

The physical mechanism powering this emission is debated (Kushnir, Katz & Waxman 2009; Cassano et al. 2010). However, a

⋆E-mail: annalisa.bonafede@hs.uni-hamburg.de
[1] We define the radio spectrum as $S(\nu) \propto \nu^{-\alpha}$.

connection with the dynamical status of the cluster is established (e.g. Buote 2001; Cassano et al. 2010).

Radio haloes are likely formed during cluster mergers, which inject a considerable amount of energy into the intracluster medium (ICM). Part of the energy is dissipated through turbulent motions and shocks. Turbulence could re-accelerate an existing population of seed relativistic electrons and produce synchrotron emission (e.g. Brunetti et al. 2001; Petrosian 2001).

Alternatively, it has been proposed that radio haloes result from inelastic hadronic collisions between cosmic-ray protons (CRp) and thermal protons (hadronic models: Dennison 1980, Blasi & Colafrancesco 1999). However, hadronic models predict γ-ray emission that has not been observed by the *Fermi* satellite (e.g. Ackermann et al. 2014). In some of the hadronic model formulations (e.g. Kushnir et al. 2009) they would require a different magnetic field in clusters with and without radio haloes, which is not observed (e.g. Bonafede et al. 011a; Govoni et al. 2010). In addition, hadronic models cannot explain radio haloes with a very steep spectral index ($\alpha > 1.5$, e.g. Brunetti et al. 2008).

Mixed hadronic and re-acceleration models have also been proposed (e.g. Brunetti & Lazarian 2011, Zandanel, Pfrommer & Prada 2014).

Although pure hadronic models cannot explain the haloes in the $L_{\rm X} - P_{1.4\,\rm GHz}$ correlation, Mpc-scale diffuse emission originating from hadronic interactions is expected in radio-off state clusters too. The first evidence for it has been found by stacking $\sim$100 images of massive clusters using the Sydney University Molonglo Sky Survey (SUMMS: Bock, Large & Sadler 1999) by Brown et al. (2011). According to Brunetti & Lazarian (2011), the electrons originating from hadronic collisions could produce radio emission that is a factor of $\sim$10 below the $L_{\rm X}$–$P_{1.4\,\rm GHz}$ correlation. The same electrons could be the seeding particles re-accelerated by turbulence during a merger.

We refer the reader to the review by Brunetti & Jones (2014) for a detailed description of the proposed mechanisms.

Recently, radio haloes have been found in clusters with low X-ray luminosities (Giovannini et al. 2011) and we have discovered the first example of a radio halo in a massive cool-core cluster that does not show signs of a recent merger (Bonafede et al. 2014). In addition, unexpected spectral features have been observed at low frequencies with early LOw-Frequency ARray (LOFAR) observations, which have detected a steepening of the radio spectrum at low frequencies in Abell 2256 (van Weeren et al. 2012). Although the spectral measure is restricted to a small portion of the halo, it indicates that more complex models – either inhomogeneous turbulence or mixed hadronic and leptonic models – have to be considered (van Weeren et al. 2012).

Before the advent of Sunyaev–Zel'dovich (SZ) large-sky surveys, X-ray catalogues were the primary source of information to 'hunt' for new radio haloes. However, due to the dependence of the X-ray luminosity on the square of the gas density, X-ray-selected samples can be biased towards low-mass and cool-core systems. As noted by Basu (2012), a better selection could be based on the SZ effect.

The SZ signal integrated over the cluster angular extent measures the total thermal energy of the gas and as such correlates closely with the total cluster mass (see *Planck* collaboration 2011, 2013 and references therein). Indeed, the SZ signal also correlates strongly with the radio power, as discovered by Basu (2012) and confirmed by Sommer & Basu (2014) and Cassano et al. (2013). After mergers, the thermalization of the gas in the ICM happens on larger timescales than the boost in X-ray luminosity, while the SZ signal will grow moderately and gradually (Sommer & Basu 2014). Hence, SZ surveys have the potential to find radio haloes in late mergers and in clusters that are left out by X-ray selections. Recently, a radio bimodality had also been found in the $P_{1.4\,\rm GHz}$–SZ plane, for clusters with $M_{500} \geq 5.5 \times 10^{14}\,{\rm M}_{\odot}$ (Cassano et al. 2013).

In this article, we present a first sample of radio observations conducted with the Giant Metrewave Radio Telescope (GMRT) with the aim of searching for new radio haloes in clusters that have a strong SZ signal. We have selected from the *Planck* catalogues published in 2011 and 2013 (Planck Collaboration et al. 2011, 2013) the most massive clusters ($M_{500} > 6 \times 10^{14}\,{\rm M}_{\odot}$) for which no radio observations were available to establish the presence of diffuse radio emission. In this article, we present the results from the first set of observations. The clusters presented in this work have been selected from the first *Planck* catalogue (Planck Collaboration et al. 2011).

The remainder of the article is as follows: in Section 2 we describe the radio observations and the main steps of the data reduction. In Section 3 we analyse the results of the observations for each cluster. A discussion of the results is presented in Section 4 and we conclude in Section 5. Throughout the article, we use a ΛCDM cosmological model with $H_0 = 71\,{\rm km\,s^{-1}\,Mpc^{-1}}$, $\Omega_{\rm m} = 0.27$, $\Omega_{\Lambda} = 0.73$.

2 RADIO OBSERVATIONS AND DATA REDUCTION

Observations were carried out at the GMRT at 325 MHz, using a 33-MHz bandwidth subdivided into 256 channels and 8 s integration time. Depending on the position of the target, the sources 3C147, 3C48 or 3C286 were observed for 15 min at the beginning of the observing block and used as absolute flux and bandpass calibrator, adopting the Scaife & Heald (2012) absolute flux scale. The absolute flux calibrators were also used to estimate the instrumental contribution to the antenna gains, which is needed for ionospheric calibration, and the instrumental phase information was used to correct the target field. In Table 1, further details about the observations are listed.

In order to obtain a uniformly reduced data sample, we have applied a semi-automated calibration procedure to the different data sets. This approach minimizes the possibility of field-dependent effects introduced by manual data reduction.

The main steps of the calibration procedure are outlined below and are based on Astronomical Image Processing System (AIPS), Source Peeling and Atmospheric Modeling (SPAM) (Intema et al. 2009) and Obit (Cotton 2008) tools. Strong radio-frequency interference (RFI) was removed from the target field data by statistical outlier flagging tools. Much of the remaining low-level RFI was modelled and subtracted from the data using Obit. After RFI removal, data sets have been averaged down to 24 channels, in order to speed up the imaging process and, at the same time, avoid significant bandwidth smearing.

For the phase calibration, we started from a model derived from the Northern Very Large Array (VLA) Sky Survey (NVSS: Condon et al. 1998) and Westerbork Northern Sky Survey (WENSS: Rengelink et al. 1997) when available. Using NVSS and WENSS, we have predicted the apparent flux of the sources at 323 MHz, using a simple spectral model fit and taking into account the GMRT primary beam. Then, a cut in flux is applied to keep only the strongest sources. Typically, 20–30 sources are included in the first model. We then proceeded with self-calibration loops. We decided not to use a phase calibrator, as the GMRT field of view is wide and a non-negligible flux is present in the field of the available phase calibrators. We note that using a phase calibrator to bootstrap the

Table 1. Radio observations.

Planck name	Alt. cluster name	Obs. date	RA and Dec. h m s, ° ′ ″	z	Scale kpc/″	Flux cal.	$\sigma_{\rm HR}$ mJy beam^{-1}	$\sigma_{\rm LR}$ mJy beam^{-1}
PSZ1 G229.70+77.97	Abell 1443	27/01/2013	12 01 27.7 +23 05 17.9	0.27	4.101	3C147	0.13	0.30
PSZ1 G086.47+15.31	CIZAJ1938.3+5409	26/01/2013	19 38 18.6 +54 09 33	0.26	3.990	3C48−3C286	0.10	0.15
PSZ1 G216.60+47.00	RXCJ0949.8+1708	25/01/2013	09 49 51.7 +17 07 08	0.38	5.175	3C147	0.15	0.20
PSZ1 G118.46+39.31	RXCJ1354.6+7715	26/01/2013	13 54 37.8 +77 15 35	0.40	5.343	3C286	0.14	0.30

Notes. Col. 1: *Planck* name; col. 2: other name from previous catalogues; col. 3: Observation date; col. 4: right ascension and declination of the target; col. 5: target redshift; col. 6: source used to set the absolute flux scale; col. 7: angular to linear scale; col. 8: root-mean-square (rms) noise in the high-resolution image; col. 9: rms noise of the low-resolution image.

flux from the absolute flux calibrator would have altered the flux scale, leading to higher errors in the flux measurements.

The first imaging steps have been performed using AIPS. In order to compensate for the non-complanarity of the array, we used the wide-field imaging technique, decomposing the GMRT field of view into ∼80–100 smaller facets, depending on the field. We performed a few rounds of cleaning and self-calibration and inspected the residual visibilities for a more accurate removal of low-level RFI. In order to correct for ionospheric effects, leading to direction-dependent phase errors, we applied SPAM calibration and imaging to the target field. The presence of strong sources in the field of view enables one to derive directional-dependent gains for each of them (similarly to the peeling technique) and to use these gains to fit a phase screen over the entire field of view. After ionospheric corrections, the last step of the calibration procedure consists of subtracting all the sources outside the central 15 arcmin from the target centre to facilitate the imaging steps.

Processed data were imaged in the Common Astronomy Software Applications package (CASA) and some more cycles of self-calibration have been performed. We have imaged the data sets at high resolution, using the Briggs weighting scheme (robust parameter equal to 0 in the CASA definition) and excluding baselines shorter than 1.1–0.9 kλ, depending on the cluster's redshift, to filter out possible emission on the Mpc scale. High-resolution (HR) images have been used to identify the radio galaxies in the cluster and to subtract their emission from the *uv* data. Specifically, we have selected the clean components corresponding to the radio galaxies detected in the HR images within 1 Mpc from the cluster centre and subtracted these clean components from the visibilities. We have used these new data sets, where the source emission had been subtracted, to search for diffuse radio emission in the clusters. To increase the brightness sensitivity to diffuse emission we have produced low-resolution (LR) images, tapering down baselines longer than 4 kλ and using the Briggs weighting scheme (robust parameter equal to 0.3 in the CASA definition).

The final images of the full field of view centred on the target were corrected for the primary beam response. We estimate that the residual amplitude errors are of the order of 10 per cent at 325 MHz, in line with the values reported for the GMRT observation at this frequency (e.g. van Weeren et al. 2009a; Intema et al. 2011; Bonafede et al. 2012).

3 INDIVIDUAL CLUSTERS

3.1 Abell 1443

Little is known about Abell 1443 in the literature. This cluster was one of the first detected by the *Planck* mission (Planck Collaboration et al. 2011). Planck Collaboration et al. (2011) report a cluster mass within r_{500}[2] of $M_{500} = 7.7^{+0.5}_{-0.6} \times 10^{14}\,{\rm M}_{\odot}$. The *ROSAT* Brightest Cluster Sample reports an X-ray luminosity $L_{[0.1\text{-}2.4\ {\rm keV}]} \sim 6.18 \times 10^{44}$ erg s^{-1} (Ebeling et al. 2000, corrected for the cosmological model used in this article). *Chandra* archival observations are also available for this target. We have retrieved the *Chandra* observations from the archive and processed them in the standard way (see Section 4). The X-ray image is shown in Fig. 1. The X-ray morphology appears elongated along the east–west direction and no defined core is clearly visible. The gas distribution, as traced by the X-ray emission, is highly perturbed, indicating that the cluster is undergoing a merger event.

As shown in Fig. 1, we detect peculiar diffuse emission in the GMRT 323-MHz image. The cluster hosts a Γ-shaped source located at ∼300 kpc from the cluster X-ray centre, which does not have the morphology of a radio galaxy (Fig. 2). Another patch of diffuse emission is located west of the Γ-shaped source (Fig. 2), located at ∼700 kpc from the cluster X-ray centre. After subtracting the sources A–G (Fig. 1, left panel), we have imaged the data at low resolution, as described in Section 2.

Extended emission is detected, as shown in the low-resolution image (Fig. 1, right panel). We note that no residual emission from sources A, B, C and D is left in the low-resolution image, indicating that the emission from the sources embedded in the diffuse emission has been properly subtracted too.

The largest linear size (LLS) of the emission is ∼1.3 Mpc. It departs from the cluster centre towards the west, encompassing the Γ-shaped source and the patch of diffuse emission, both detected in the high-resolution image. Because of its peculiar morphology, a classification of this emission into the usual halo and relic categories is not straightforward. The western patch of diffuse emission could be a relic, as it is at the edge of the X-ray emission and has an LLS of ∼660 kpc. Given its morphology and the fact that no component is visible in the *Wide-Field Infrared Survey Explorer* (*WISE*) 3.4 image (Fig. 1, Wright et al. 2010), the possibility that we are seeing a radio galaxy is less convincing.

The emission located centrally could instead be classified as a radio halo, as it has an LLS of ∼1.1 Mpc. However, the emission itself is peculiar because of its morphology and it contains a bright Γ-shaped source. In another case (MACSJ0717+3745: Bonafede et al. 2009, van Weeren et al. 2009b), a brighter part, possibly a relic or a bright filament, has been found embedded in the radio halo emission. Spectral index and polarization information are needed to distinguish the origin of the Γ-shaped source and understand the nature of the entire diffuse emission. Details about the radio properties of the emission detected in this cluster are listed in Table 2.

[2] r_{500} is defined as the radius at which the cluster density is 500 times the critical density.

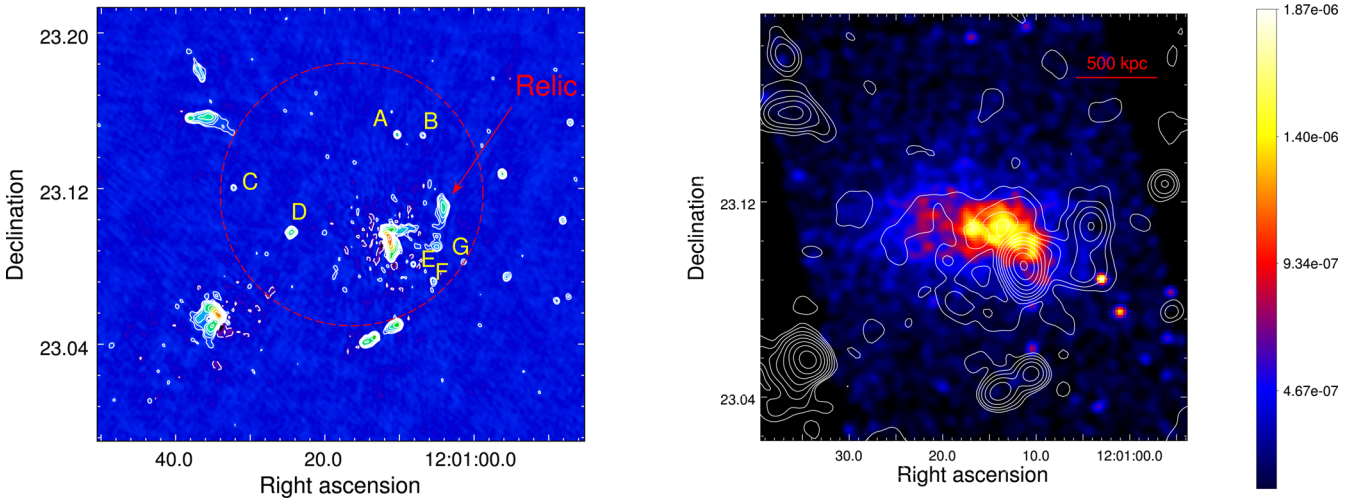

Figure 1. Abell 1443. Left panel: HR image at 323 MHz in greyscale and isobrightness contours. The beam is 9.8 × 8.1 arcsec^2. Contours start at 0.5 mJy beam^{-1} and are spaced by a factor of 2. The first negative contour is dashed. The red dashed circle is centred on the X-ray centre of the cluster and has a radius of 1 Mpc. The sources subtracted in the LR image are marked by letters (A to G). Right panel: greyscale: exposure-corrected X-ray emission of the cluster from *Chandra* in the 0.5–7 keV energy range. The colour bar has units of photon cm^{-2} s^{-1} pixel^{-1}. Radio isobrightness contours from the radio LR image are overplotted. The beam is 27.4 × 26.7 arcsec^2. Contours start at 1.1 mJy beam^{-1} and are spaced by a factor of 2. The first negative contour is dashed. [A colour version is available in the on-line version.]

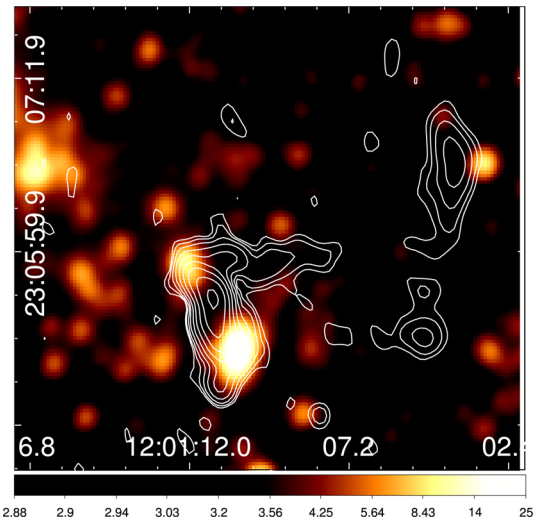

Figure 2. Zoomed view of the Γ-shaped source and relic region of A1443. The contours are the same as in Fig 1. Left panel: greyscale refer to the *WISE* 3.4-μm image. The colour bar is in magnitudes, not calibrated in terms of absolute surface brightness. [A colour version is available in the on-line version.]

To verify that the diffuse emission is not affected by the incomplete subtraction of the sources detected at high resolution (A–G in Fig. 1), we have convolved the residual of the high-resolution image with a Gaussian having the same major and minor axis as the restoring beam of the LR image (Fig. 3). In this image, the HR contours are plotted over the LR ones and over the contours of the residuals of the HR image convolved at low resolution. From this image, we conclude that the sources A, B, C, D and F are properly subtracted. Some residual is detected corresponding to the position of source G, on top of the relic. This emission contributes 0.2 mJy to the relic emission. Therefore, it does not affect our estimate of the relic flux density.

3.2 CIZAJ1938.3+5409

The cluster CIZAJ1938.3+5409 is located in the so-called '*zone of avoidance*' and was discovered by Ebeling et al. (2002) by inspecting X-ray data from the *ROSAT* All-Sky Survey (RASS) Bright Source Catalogue (Ebeling et al. 2000). The authors report an X-ray luminosity of $L_{[0.1\text{-}2.4\,\mathrm{keV}]} \sim 10.89 \times 10^{44}$ erg s^{-1} (corrected for the cosmological model adopted in this work). The cluster mass, as reported by *Planck* (Planck Collaboration et al. 2013), is $M_{500} = 7.5^{+0.4}_{-0.3} \times 10^{14}\,\mathrm{M}_{\odot}$. Therefore it is quite a massive

Table 2. Radio sources.

Planck name	Other name	Detection	Flux density mJy	Radio power at 323 MHz W Hz^{-1}	LAS × SAS arcsec × arcsec	LLS × SLS kpc × kpc
PSZ1 G229.70+77.97	Abell 1443	Whole emission	580 ± 59	1.4 ± 0.1 × 10^{26}	330 × 230	1350 × 940
		Halo(?)	74.0 ± 7.6	1.7 ± 0.2 × 10^{25}	270 × 230	1100 × 940
		Relic(?)	57.0 ± 5.8	1.3 ± 0.1 × 10^{25}	160 × 65	660 × 270
		Γ-shaped source	450 ± 45	1.1 ± 0.1 × 10^{26}	100 × 60	410 × 250
PSZ1 G086.47+15.31	CIZAJ1938.3+5409	Halo	11.0 ± 1.2	2.4 ± 0.3 × 10^{24}	180 × 100	720 × 400
PSZ1 G216.60+47.00	RXCJ 0949.8+1708	Halo	21.0 ± 2.2	1.1 ± 0.1 × 10^{25}	200 × 80	1040 × 400

Notes. Col. 1: *Planck* name; col. 2: other name from previous catalogues; col. 3: extended source detected in the cluster; col. 4: flux density of the detected source or upper limit to it; col. 5: radio power of the detected source, assuming a spectral index $\alpha = 1.3$ for the k correction; col. 6: largest and smallest angular scale of the source; col. 7: largest and smallest linear scale of the source in the adopted cosmological model.

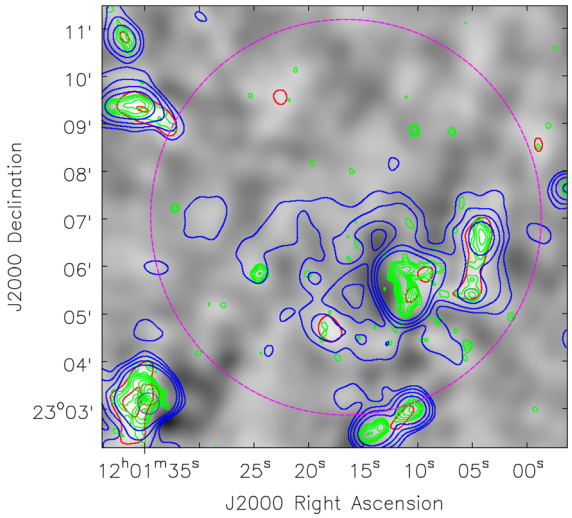

Figure 3. A1443. Grey colour scale: LR image of the cluster, blue contours as in Fig. 1, right panel. Green contours are as in Fig. 1, left panel. Red contours are the residual of the HR image convolved with a beam like the one of the LR image. Red contours are drawn at $\pm 3\sigma$. The dashed circle is centred on the cluster centre and has a radius of 1 Mpc. The restoring beams are shown in the bottom left corner. [A colour version is available in the on-line version.]

cluster, but unfortunately nothing is known in the literature about its dynamical state.

Chandra observations are available for this target (Jones et al., in preparation). The X-ray and radio emission of the cluster are shown in Fig. 4.

After source subtraction, we discover extended radio emission, located at the cluster centre and having a size of ∼720 kpc (Fig. 4, left panel). The flux density of the emission is 11 mJy, which translates into a power of $2.4 \pm 0.3 \times 10^{24}$ W Hz^{-1} at 323 MHz. The size and position of the emission would classify it as a radio halo. We note that the corresponding power at 1.4 GHz would be $P_{1.4\,\mathrm{GHz}} \sim 4 \times 10^{23}$ W Hz^{-1}, which is unusually low for such a massive cluster.[3] Indeed, the halo is at least 8–10 times underluminous in radio for its SZ signal and X-ray power, respectively (see Fig. 12 later). The radio power at 1.4 GHz would place the halo in the 'upper-limit' region of the $P_{1.4\,\mathrm{GHz}}$–M_{500} plane.

To verify that the diffuse emission is not due to the incomplete subtraction of the sources detected at high resolution (A–H in Fig. 4), we have convolved the residual of the high-resolution image with a Gaussian having the same major and minor axis as the restoring beam of the LR image (Fig. 5). In this image, the HR contours are plotted over the LR ones and over the contours of the residuals of the HR image convolved at low resolution. From this image, we conclude that the sources A, B, C, D, F, G and H are properly subtracted, as no residual emission is detected in either the LR image or the residual image. Some residual emission is detected corresponding to source E. This emission accounts for 0.2 mJy and is confined only to the source position, hence it cannot explain the 11-mJy emission on a larger scale detected in the LR image.

3.3 RXCJ 0949.8+1708

The cluster RXCJ 0949.8+1708, also known as MACS J0949.8+1708, is an X-ray-luminous cluster, discovered in X-rays by the *ROSAT* satellite (Ebeling et al. 2000). The *Planck* satellite detected the cluster through the SZ effect (Planck Collaboration et al. 2011) and found it to be massive, with $M_{500} = 8.2 \pm 0.6 \times 10^{14}$ M$_\odot$ (Planck Collaboration et al. 2013).

Ebeling et al. (2010) have analysed the cluster in detail using the University of Hawaii 2.2-m optical telescope and X-ray *Chandra* observations. They derive an X-ray luminosity $L_{\mathrm{X}[0.1-2.4\,\mathrm{keV}]} = 10.6 \pm 0.6 \times 10^{44}$erg s^{-1} within R_{500} and a temperature $T = 8.9 \pm 1.8$ keV.

In Fig. 6, the X-ray emission of the cluster is shown. The MACS clusters in Ebeling et al. (2010) have been classified with a morphological code from 1 to 4, with 1 meaning pronounced cool-core and good optical–X-ray alignment and 4 meaning multiple X-ray peaks and no cD galaxy. RXCJ 0949.8+1708 is given a morphological code 2, meaning that, although no pronounced cool core is present, the X-ray emission shows a good optical–X-ray alignment and concentric X-ray contours.

This cluster has already been observed by Venturi et al. (2008) at 610 MHz (the author refer to the cluster with the name Z2261), who found positive residuals after the subtraction of the sources and indicated the cluster as a candidate radio halo.

In Fig. 6, the radio image from our new GMRT observations is shown. We detect diffuse radio emission located at the cluster centre and with an LLS of ∼1 Mpc, confirming that the positive residuals detected by Venturi et al. (2008) are part of more extended radio emission. We classify the emission as a radio halo. It is elongated in the southwest–northeast direction and does not follow the emission of the gas.

To verify that the diffuse emission is not affected by the incomplete subtraction of the sources detected at high resolution (A–H in Fig. 6), we have convolved the residual of the high-resolution image with a Gaussian having the same major and minor axis as the restoring beam of the LR image (Fig. 7). From this image we conclude that the sources are properly subtracted. Some residual is detected on top of the brightest region of the halo. Likely, it is the brightest part of the radio halo, which is on a scale smaller than 1 Mpc and, as such, is not filtered out in the HR image. The flux density corresponding to this emission is ∼0.5 mJy; hence, even if it came from the individual radio sources, it would not affect the estimate of the halo flux density (see Table 2).

3.4 RXCJ1354.6+7715

RXCJ1354.6+7715, also known as MACS J1354.6+7715, is an X-ray-luminous galaxy cluster discovered by Böhringer et al. (2000). They report an X-ray luminosity in the energy band 0.1–2.4 keV of $L_{\mathrm{X}[0.1-2.4\,\mathrm{keV}]} = 9.4 \times 10^{44}$erg s^{-1} (corrected for the cosmological model used in this work).

The *Planck* satellite detected the cluster through the SZ effect (Planck Collaboration et al. 2011). Planck Collaboration et al. (2013) report $M_{500} = 6.2 \pm 0.6 \times 10^{14}$ M$_\odot$.

Horesh et al. (2010) have analysed the matter substructure in the cluster using strongly lensed arcs detected through *Hubble* Space Telescope (HST) observations. Their analysis suggests the existence of two separate galaxy concentrations. They conclude that this cluster could be during some stage of a merger, with a considerable amount of substructure.

Chandra observations are available in the archive. We have calibrated them in the standard way (see Section 4) and in Fig. 8 the X-ray emission is shown. In agreement with the optical analysis by Horesh et al. (2010), two gas concentrations are clearly detected.

[3] We assume $\alpha = 1.2$.

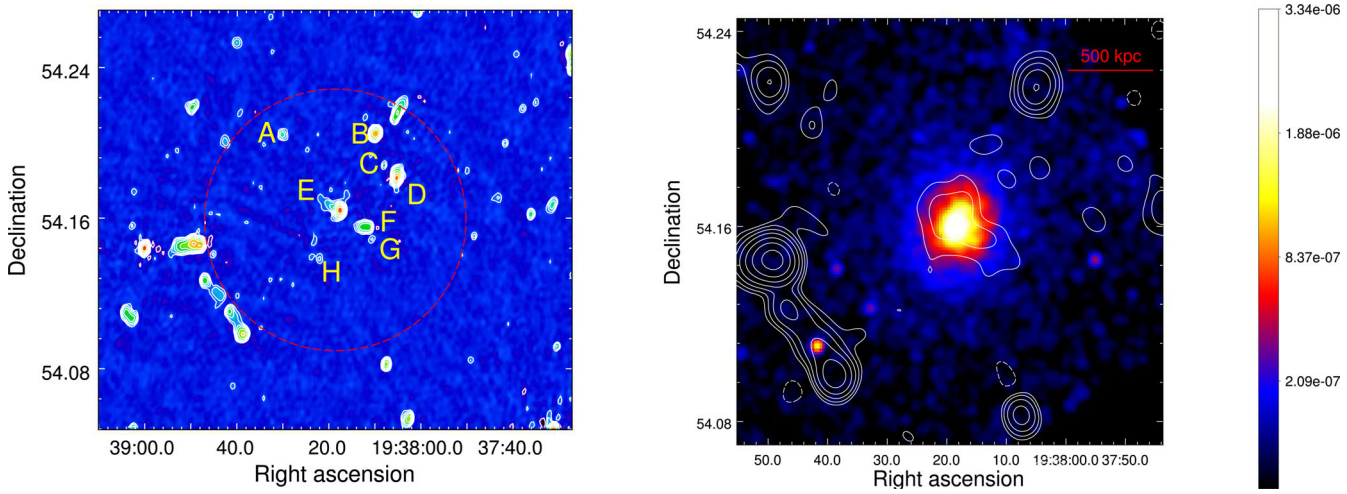

Figure 4. CIZAJ1938.3+5409. Left panel: HR image at 323 MHz in geyscale and isobrightness contours. The beam is 12.9 × 8.8 arcsec^2. Contours start at 0.3 mJy beam^{-1} and are spaced by a factor of 2. The first negative contour is dashed. The red dashed circle is centred on the X-ray centre of the cluster and has a radius of 1 Mpc. The sources subtracted in the LR image are marked by letters (A to H). Right panel: X-ray emission of the cluster from *Chandra* in geyscale and isobrightness contours from the radio LR image. The colour bar has units of photon cm^{-2} s^{-1} pixel^{-1}. The beam is 40.3 × 34.9 arcsec^2. Contours start at 0.7 mJy beam^{-1} and are spaced by a factor of 2. The first negative contour is dashed. [A colour version is available in the on-line version.]

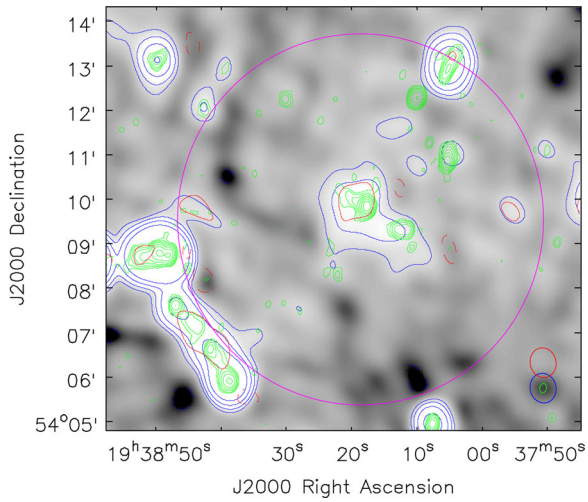

Figure 5. CIZAJ1938.3+5409. Grey colour scale: LR image of the cluster, blue contours as in Fig. 4, right panel. Green contours as in Fig. 4, left panel. Red contours are the residual of the HR image convolved with a beam like the one of the LR image. Red contours are drawn at ±3σ. The dashed circle is centred on the cluster centre and has a radius of 1 Mpc. The restoring beams are shown in the bottom right corner. [A colour version is available in the on-line version.]

In Fig. 8 the radio emission from the cluster at 323 MHz is shown. A bright radio galaxy (C in Fig. 8, left panel) is located at the centre of the cluster. Its total flux is ∼159 mJy. It has a nucleus and a lower surface brightness tail. Residual calibration errors are present around the radio galaxy. The presence of the tail and the residual calibration errors make subtraction of the clean components of the radio galaxy C difficult.

Some residual emission is present in the low-resolution radio image, which is likely due to the convolution at lower resolution of the residual calibration errors of the radio galaxy C and residual emission from the tail. In order to confirm this, we have convolved the residuals obtained after the cleaning of the high-resolution image with a Gaussian having the same major and minor axis as the restoring beam of the low-resolution image. The comparison is shown in Fig. 9. Hence, despite the massive and likely merging cluster, no radio emission in the form of a radio halo or relic is present at the sensitivity level reached by our observations.

It must be noted that RXCJ1354.6+7715 is the least massive cluster among those analysed in this article. Putting an upper limit to the possible radio emission below our detection threshold is not trivial, because of the presence of residual calibration errors connected with radio galaxy C and more generally because of the non-universal surface brightness distribution of radio haloes. However, considering a conservative detection threshold of $3\sigma_{\rm LR}$ over a circle of 350 kpc radius, we can exclude the presence of radio emission on a scale ≥700 kpc with a flux density $S \sim 5$ mJy, which translates into an upper limit of $P_{1.4\,\rm GHz} < 5 \times 10^{23}$. This value is a factor of ∼5 below the $P_{1.4\,\rm GHz}$–SZ correlation.

4 DISCUSSION

4.1 Substructure analysis

All the clusters analysed in this work have *Chandra* archival observations. X-ray images are a powerful tool to understand the cluster dynamical state, complementary to optical observations.

We have reprocessed the *Chandra* observation of the clusters using the latest calibration tables (CALDB 4.5.9) in Chandra Interactive Analysis of Observations. Following Cassano et al. (2010), the event files have been binned by a factor of four in order to undersample the *Chandra* PSF. We have selected the 0.5–2 keV energy band and we have verified that more than 2000 counts were detected inside the region of interest (a circle of 500 kpc radius) to allow for morphological analysis. The images have been normalized by the exposure map and the sources in the cluster field have been identified visually and excluded from the analysis.

In order to quantify the dynamical status of the clusters, we compute three dynamical indicators, extensively used in the literature (e.g. Böhringer et al. 2010): the power ratio P_3/P_0, the centroid shift w and the concentration parameter c.

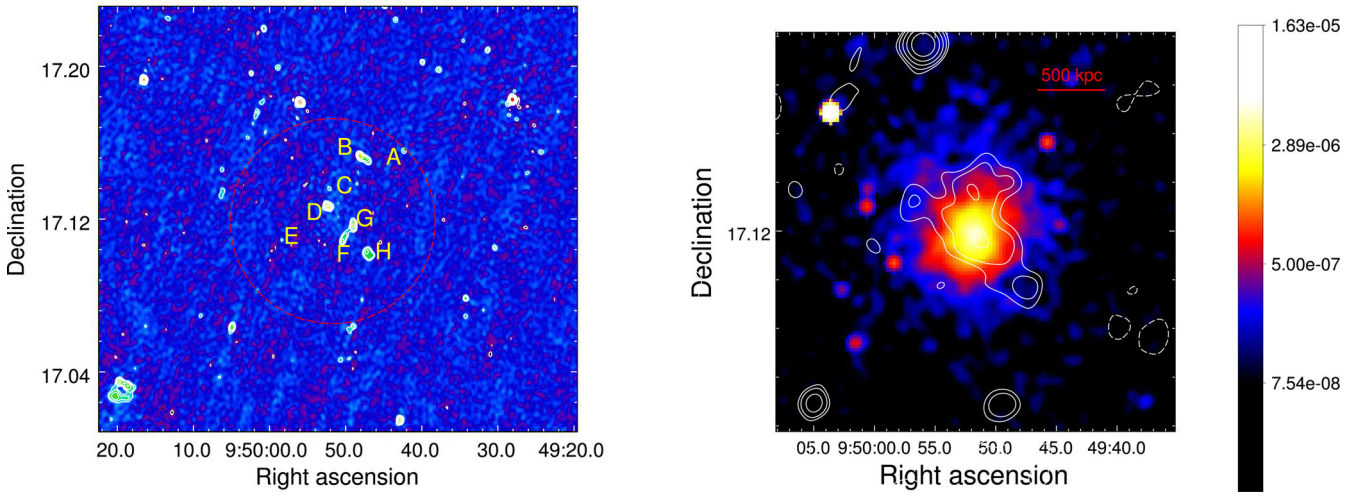

Figure 6. RXCJ0949.9+1708. Left panel: HR image at 323 MHz in greyscale and isobrightness contours. The beam is 9.8 × 7.9 arcsec^2. Contours start at 0.5 mJy beam^{-1} and are spaced by a factor of 2. The first negative contour is dashed. The red dashed circle is centred on the X-ray centre of the cluster and has a radius of 1 Mpc. The sources subtracted in the LR image are marked by letters (A–H). Right panel: X-ray emission of the cluster from *Chandra* (Ebeling et al. 2010) in greyscale and isobrightness contours from the radio LR image. The colour bar has units of photon cm^{-2} s^{-1} pixel^{-1}. The beam is 27.2 × 26.8 arcsec^2. Contours start at 0.7 mJy beam^{-1} and are spaced by a factor of 2. The first negative contour is dashed. [A colour version is available in the on-line version.]

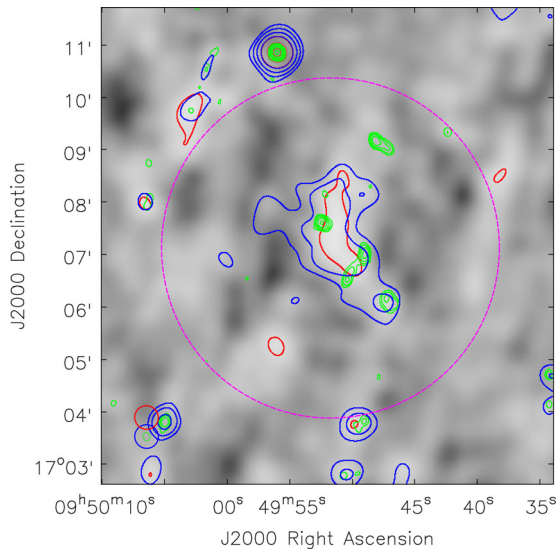

Figure 7. RXCJ0949+1708. Grey colour scale: LR image of the cluster, blue contours as in Fig. 6, right panel. Green contours as in Fig. 6, left panel. Red contours are the residual of the HR image convolved with a beam like the one of the LR image. Red contours are drawn at ±3σ. The dashed circle is centred on the cluster centre and has a radius of 1 Mpc. The restoring beams are shown in the bottom left corner. [A colour version is available in the on-line version.]

Cassano et al. (2010) have used these methods, finding that clusters with and without radio haloes occupy different regions in the morphological diagrams. Recently, we have found a first outlier (Bonafede et al. 2014) in the case of CL1821+643.

The morphological indicators P_3/P_0, w and c have been computed within an aperture radius $R_{ap} = 500$ kpc and considering as centre the centroid of the X-ray emission (P_3/P_0 computation) and the cluster X-ray peak (c and w computation), in order to have a fair comparison with the clusters analysed by Cassano et al. (2010). We note that the clusters presented in this work have mass and redshift comparable to the clusters analysed by Cassano et al. (2010), hence the comparison makes sense. The errors and the photon bias have been estimated through Monte Carlo simulations, following the approach of Böhringer et al. (2010).

The centroid shift method (Maughan et al. 2008) measures the standard deviation of the projected separation between the X-ray peak and the centroid in units of R_{ap}, computed within circles of increasing radius (from 0.05 R_{ap} to R_{ap}, in steps of 0.05 R_{ap}). The centroid shift, w, has been derived computing the X-ray-weighted centroid within circles of increasing radius.

The concentration parameter, c, measures the ratio between the X-ray surface brightness within 100 kpc and the surface brightness within 500 kpc (Santos et al. 2008). It is higher for cool-core and regular clusters, while it is lower for merging clusters.

The power ratio is a multipole decomposition of the two-dimensional projected mass distribution (Buote & Tsai 1995). We have determined the power ratio P_3/P_0, which is the lowest power-ratio moment providing a clear substructure measure. Following Böhringer et al. (2010), momenta are computed excising the inner $0.05\times R_{ap}$. In the computation of P_3/P_0, the photon bias takes into account the spurious amount of substructure that could contribute to the power ratio. As noted by Böhringer et al. (2010), very regular clusters would also show some substructure because of photon noise. Since we are comparing results here with the analysis by Cassano et al. (2010), the bias will not be taken into account in the following analysis. However, the photon bias gives a larger contribution to regular clusters than to perturbed ones. Hence, once it is taken into account in the power ratio analysis, the separation of merging and regular clusters along the P_3/P_0 axis would likely be more evident.

In Fig. 11, we show the positions of the clusters in the $P_3/P_0 - c$ and $w - c$ diagrams, taken from Cassano et al. (2010) and Bonafede et al. (2014).

4.1.1 Abell 1443

The substructure analysis confirms the visual impression from the X-ray image. We obtain $w = 0.0406 \pm 0.004$, $c = 0.112 \pm 0.006$

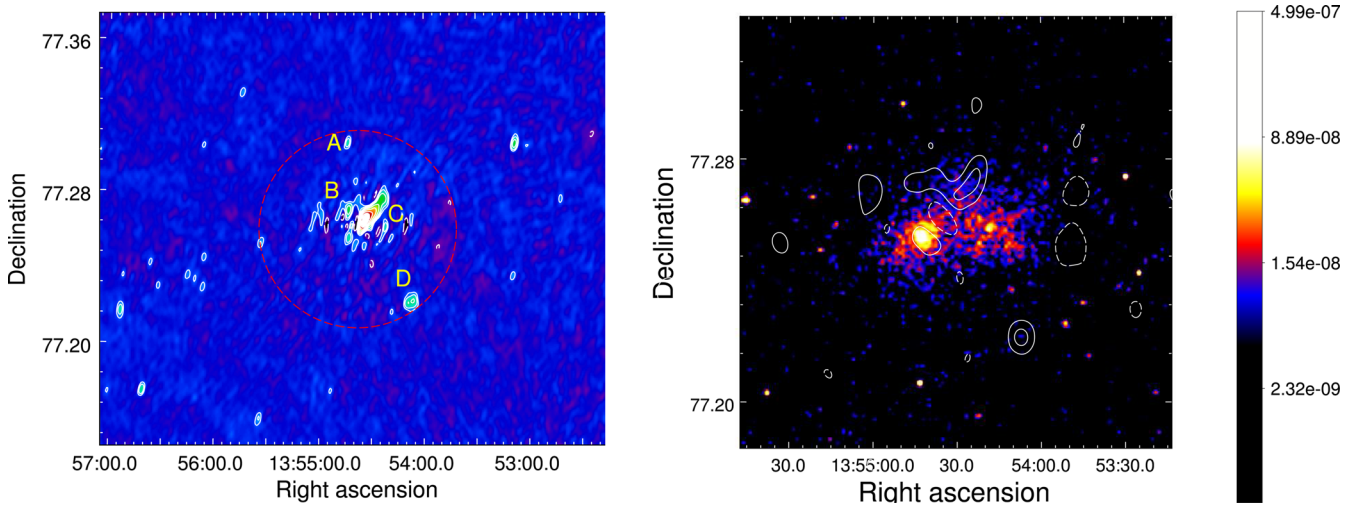

Figure 8. RXCJ1354.6+7715. Left panel: HR image at 323 MHz in greyscale and isobrightness contours. The beam is 19.4 × 878 arcsec^2. Contours start at 0.5 mJy beam^{-1} and are spaced by a factor of 2. The first negative contour is dashed. The red dashed circle is centred on the X-ray centre of the cluster and has a radius of 1 Mpc. The sources subtracted in the LR image are marked by letters (A–D). Right panel: X-ray emission of the cluster from *Chandra* 0.5–2 keV energy band in greyscale and isobrightness contours from the radio LR image. The colour bar has units of photon cm^{-2} s^{-1} pixel^{-1}. The beam is 33.7 × 25.6 arcsec^2. Contours start at 0.8 mJy beam^{-1} and are spaced by a factor of 2. The first negative contour is dashed. [A colour version is available in the on-line version.]

and $P_3/P_0 = (1.6 \pm 0.7) \times 10^{-6}$. The dynamical status of the cluster is highly perturbed and the cluster falls in the merging quadrant of the $P3 - P0$, w, c diagrams.[4] As expected for such massive and merging clusters, diffuse radio emission has been discovered.

4.1.2 *CIZAJ1938.3+5409*

We obtain an upper limit for the value of $P_3/P_0 < 3.8 \times 10^{-8}$ and a rather high value of $c = 0.292 \pm 0.006$, which are typical for non-merging clusters. In contrast, the shift parameter $w = 0.040 \pm 0.003$ is typical of merging clusters. Although a major merger can reasonably be excluded, the analysis is not conclusive regarding the cluster dynamical status.

In Fig. 11, the cluster position in the morphological planes is shown. We note the peculiar position of the cluster in the diagrams. While in the plane $c - P_3/P_0$ the clusters sits among the non-merger ones, it lies in an almost empty quadrant in the $c - w$ and $w - P_3/P_0$ planes.

We note that the cluster morphological indicators are very similar to those of CL1821+643 (Bonafede et al. 2014). However, the radio emission in the two clusters is rather different. CL1821+643 hosts a radio halo with a power that follows the $P_{1.4\,\mathrm{GHz}}$–L_X and $P_{1.4\,\mathrm{GHz}}$-SZ correlations, while the radio halo discovered in CIZAJ1938.3+5409 has a radio power at least eight times lower than the $P_{1.4\,\mathrm{GHz}}$-SZ correlations.

Recently, Khatri (2015) has shown that *Planck* SZ measurements might be contaminated by CO Galactic emission. This would result in an overestimate of the cluster mass from SZ measurements, which can be relevant for clusters close to the Galactic plane. In the case of CIZAJ1938.3+5409, a mass $M_{500} \sim 4 \times 10^{14}\,\mathrm{M}_\odot$ would bring the radio halo on to the $P_{1.4\,\mathrm{GHz}}$-SZ correlation. As the errors in *Planck* masses are not quantified yet, a more precise estimate of the possible error in this cluster cannot be derived. However, we note that the cluster does not fall in the most CO-contaminated regions derived by Khatri (2015). This suggests that the mass derived by *Planck* is a good estimate of the cluster mass.

[4] As expected, in this case the bias would not change the value of P_3/P_0 dramatically. Taking the photon bias into account, one would obtain $P_3/P_0 = (1.5 \pm 0.7) \times 10^{-6}$.

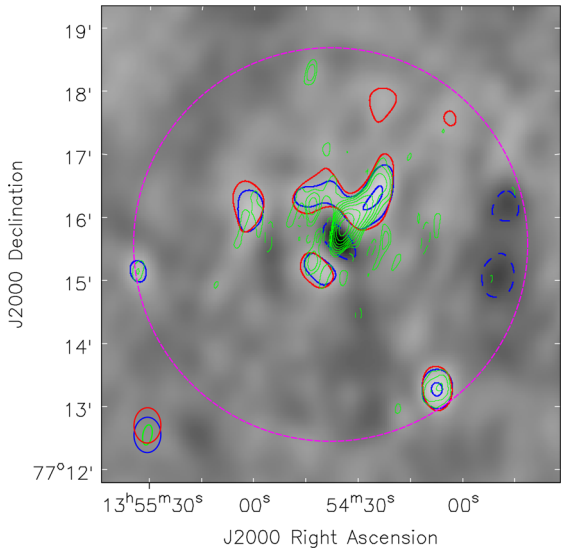

Figure 9. RXCJ1354.6+7715. Grey colour scale: LR image of the cluster, blue contours as in Fig. 4, right panel. Green contours as in Fig. 4, left panel. Red contours are the residual of the HR image convolved with a beam like the one of the LR image. Red contours are drawn at $\pm 3\sigma$. The dashed circle is centred on the cluster centre and has a radius of 1 Mpc. In the bottom left corner, the restoring beams are plotted. [A colour version is available in the on-line version.]

Since the cluster total luminosity in the band 0.1–2.4 keV is known (Ebeling, Mullis & Tully 2002, see Section 3.2), we have checked the position of the radio halo in the $P_{1.4\,\mathrm{GHz}}$–L_X plane (Kale et al. 2015). Also in this diagram the radio halo is a factor ∼10 below the $P_{1.4\,\mathrm{GHz}}$–L_X correlation and falls in the upper-limit region. This provides independent evidence – with respect to the *Planck* mass

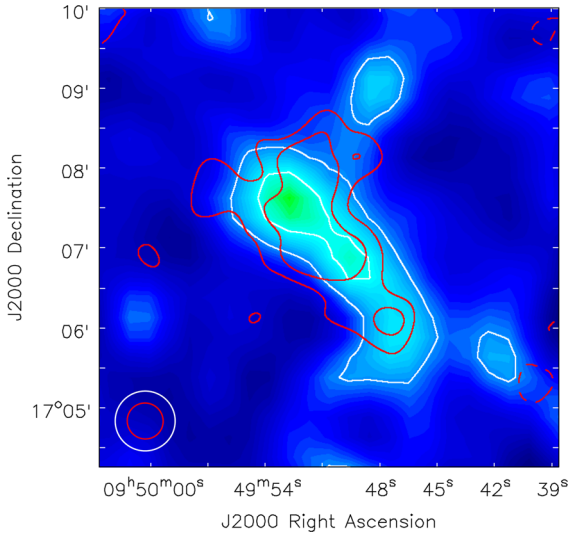

Figure 10. RXCJ0949.9+1708. Greyscale and white contours refer to the emission at 1.4 GHz from the NVSS. White contours are drawn at (−1, 1, 2, 4) mJy beam^{-1}. The beam is 45 × 45 arcsec^2. The first negative contour is dashed. Red contours refer to the LR GMRT image (as in Fig. 6, right panel). [A colour version is available in the on-line version.]

measurement – that the cluster hosts a radio halo of low power for its mass.

In the next section, we discuss the possible origin for the low-power radio halo in CIZAJ1938.3+5409.

4.1.3 RXCJ0949.9+1708

For RXCJ0949.8+1708, the morphological analysis is not conclusive regarding the cluster dynamical status. We obtain $w = 0.0113 \pm 0.003$, $c = 0.197 \pm 0.007$ and $P_3/P_0 = (3.8 \pm 3.6) \times 10^{-7}$. As can be seen from Fig. 11, w and c are at the edge of the quadrant among radio-quiet and radio-loud clusters and so is P_3/P_0, within the error. We note that if the bias was taken into account in the P_3/P_0 computation, we would only be able to put an upper limit $P_3/P_0 < 3.5 \times 10^{-7}$.

The cluster sits in the central regions of the morphological diagrams, in between regular and merging clusters. The values of w, c, P_3/P_0 and the presence of a BGC at the cluster centre suggest that no major merger is occurring. However, present data do allow us to exclude a major merger along the line of sight. Additional optical or weak lensing data are required to assess the cluster dynamical status.

We have estimated the spectral index of the halo in RXCJ0949.8+1708 using NVSS and VLA Low-Frequency Sky Survey Redux Source Catalog (VLSSr: Lane et al. 2014) images. In Fig. 10, the radio emission from NVSS is shown, superimposed on to the GMRT LR image. We have estimated the spectral index in the region where both images have signal above three times the noise. Since it is not possible to estimate the contribution of the sources (A–H in Fig. 6) in the NVSS image, only an upper limit to the halo flux can be derived. Since no emission is present in the VLSSr image above three times the noise, we have put an upper limit on the halo flux. Assuming that the spectrum is described by a single power law between 74 MHz and 1.4 GHz, we can constrain the spectral index in the range $0.6 < \alpha < 1.5$. Hence, we can only exclude a very steep-spectrum radio halo.

4.1.4 RXCJ1354.6+7715

The results from the substructure analysis are $P_3/P_0 = (4 \pm 1) \times 10^{-6}$, $w = 0.080 \pm 0.004$ and $c = 0.201 \pm 0.006$, which places the cluster among the merging ones, although the high value of c indicates that the core has not been disrupted by the merger. Alternatively, the high value of c could indicate a second merger along the line of sight. These results are in agreement with the optical analysis by Horesh et al. (2010).

No radio halo is detected at the sensitivity threshold of our observations and, under some assumptions (see Section 3), we cannot exclude the presence of diffuse radio emission at a level a factor of five below the $P_{1.4\,\mathrm{GHz}}$-SZ correlation.

4.2 CIZAJ1938.3+5409: the first hadronic halo?

The radio halo discovered in CIZAJ1938.3+5409 is the first direct detection of radio emission in a radio-off state cluster. As it is at least eight times underluminous in radio for its SZ signal, we discuss two possibilities for the origin of the radio emission.

(i) The observed emission in CIZAJ1938.3+5409 could be due to secondary electrons originating from hadronic interactions between thermal and non-thermal protons (Pfrommer & Enßlin 2004b; Enßlin et al. 2011). We note that the mentioned works aimed at explaining radio haloes with a higher power than the one observed in CIZAJ1938.3+5409. However, they can easily be extrapolated at lower radio powers, because the particle spectrum predicted by the models is a simple power law. The extrapolation at lower radio power has already been performed, e.g. by Brunetti & Lazarian (2011). According to this work, the electrons originating from hadronic collisions could produce radio emission that is a factor of ∼10 below the L_X–$P_{1.4\,\mathrm{GHz}}$ correlation. *Fermi* upper limits indicate that the ratio of non-thermal CR protons to thermal energy densities is lower than a few per cent (Ackermann et al. 2014).

Stacking a sample of clusters in radio, Brown et al. (2011) have claimed the first detection of the radio-off state of clusters. In order to understand better the possibility that this halo is produced by secondary electrons, we have investigated a set of simple models for CIZAJ1938.3+5409. As a first approximation, we have assumed a β model for the gas density, rescaled to the mass of the cluster. We have assumed an isothermal temperature of $T \approx 6.4$ keV as indicated by X-ray data and we have computed the profile of cosmic-ray (CR) protons by requiring that the energy in CR is a fixed fraction of the gas energy, ϵ_{CR}.

Furthermore, we have modelled the magnetic field of the cluster as was done in Bonafede et al. (2013). Specifically, we have generated a power-law spectrum distribution of vector potential in Fourier space for a 200^3 grid, randomly drawn from the Rayleigh distribution, and we have computed the magnetic field in real space as $B = \nabla \times A$, ensuring $\nabla \cdot B = 0$ by construction. We have assumed that the maximum coherence scale of the magnetic field is 34 kpc, the power law of fluctuations is a Kolomogorv spectrum and the average magnetic field strength in the central Mpc^3 is $\langle B \rangle = 2\,\mu$G, as found for Coma (Bonafede et al. 2010).

Since the radio spectrum of the halo is not well constrained, we explore a few possibilities for the spectrum of cosmic-ray protons and adjust the energy budget of CRs so that the secondary radio emission matches our observation. We compute the hadronic γ-ray emission following Pfrommer & Enßlin (2004a) and Donnert et al. (2010), with the only difference that for the hadronic cross-section we use the parametrization of the proton–proton cross-section given by Kelner, Aharonian & Bugayov (2006); see also Vazza et al.

Table 3. Parameters of our models of hadronic secondary emission for PSZ1 G086.47+15.31, always assuming a Coma-like magnetic field configuration, with $\langle B \rangle = 2$ μG in the central Mpc^3. See text for details.

Model	p	α	ϵ_{CR}	$P_{325\,MHz}$ [W Hz^{-1}]	$P_{0.5\text{-}100\,GeV}$ [erg s^{-1}]	$F_{0.5\text{-}100\,GeV}$ [photon (cm^2 s)$^{-1}$]
1	−3.1	1.7	0.91	2.4×10^{24}	5.2×10^{42}	3.9×10^{-10}
2	−2.9	1.6	0.13	2.4×10^{24}	8.5×10^{41}	6.5×10^{-11}
3	−2.7	1.5	0.018	2.4×10^{24}	1.4×10^{41}	1.1×10^{-11}
4	−2.5	1.3	0.0093	2.4×10^{24}	2.3×10^{40}	1.7×10^{-12}
5	−2.3	1.2	0.0004	2.4×10^{24}	3.6×10^{39}	2.7×10^{-13}
6	−2.1	1.1	0.0001	2.4×10^{24}	5.5×10^{38}	4.2×10^{-14}

(2015) for details. The secondary emission is based on Dolag & Enßlin (2000).

Results are listed in Table 3. All models with a spectrum of CRs $p \leq -3$ (with $dN/dE \propto E^p$) produce hadronic emission below the deepest limits by *Fermi*, which are at the level of $\sim 10^{-10}$ photon/(cm^2 s) (e.g. Huber et al. 2013; Ackermann et al. 2014). The model with $p = -3.1$ produces emission above the detectability of *Fermi*. However, the energy budget of CRs nearly equals the thermal energy, making the model unrealistic.

A direct observation of this cluster with *Fermi* is impractical, due to its location in the Zone of Avoidance. Our calculations suggest that a hadronic origin for the radio halo in CIZAJ1938.3+5409 is consistent with the current *Fermi* limits. However, we note that if the cluster was at the luminosity distance of Coma ($\sim$ 99 Mpc) then it should be detected in γ-rays only if $p \leq -2.3$, i.e. $\alpha \geq 1.2$. These estimates must be taken as approximate, because of the uncertainties in both magnetic field distribution and strength, which translate into an uncertainty in the normalization of the energy budget of CRs for a given spectrum. For instance, for a magnetic field $\langle B \rangle = 0.1$ μG, *Fermi* upper limits would be violated for $p = -2.1$.

Our calculations suggest that, if the halo has a hadronic origin, some clusters of the same mass as CIZAJ1938.3+5409 in the nearby Universe might host radio and γ-ray emission just above the current level of detectability. These haloes do not represent the classic giant radio halo population, but rather a much broader population of 'radio-quiet' objects that still need to be detected.

(ii) The second possibility to explain the radio emission in CIZAJ1938.3+5409 is that we are observing a radio halo in its rapid transition phase between the upper-limit region and the $P_{1.4\,GHz}$–SZ correlation. A direct test, as done for the hadronic origin of the radio emission above, is not possible here because of the many free parameters. However, we can make some statistical considerations in order to establish whether the low-power radio halo could be due to the same mechanism that powers radio haloes in the $P_{1.4\,GHz}$–SZ correlation.

In the framework of re-acceleration models, merger-induced turbulence lights up the radio emission, lifting the clusters from the radio-off state region of the $P_{1.4\,GHz}$–SZ plane up to the radio-on state of the $P_{1.4\,GHz}$–SZ correlation. The steepest spectrum radio haloes are expected to be below the correlation, as they represent the latest stage of radio halo life (Donnert et al. 2013). The halo in CIZAJ1938.3+5409 could be in the very early or very late stage of its radio-on phase. In both cases, its spectrum should be steep ($\alpha \geq 1.5$). As no emission is detected in the VLSSr image, we can only put an upper limit on the spectral index, $\alpha < 1.9$. We cannot exclude the possibility that the radio halo has a very steep spectrum and that we are observing it just before it enters its radio-off state. According to the simulations by Donnert et al. (2013), clusters should spend $\sim$0.1–0.2 Gyr in the region of the $P_{1.4\,GHz}$–L_X plane between the upper limits and the radio power measured for CIZAJ1938.3+5409. Clusters as massive as CIZAJ1938.3+5409 formed $\approx$6 Gyr ago (Giocoli et al. 2007). Hence, assuming that all the clusters follow the same path in the $P_{1.4\,GHz}$–L_X plane, one would expect to find at maximum one cluster in $\approx$20–40 objects of the same mass and at the same redshift in the transition region, which is not at odds with current statistics. A proper estimate should account for the different merging rate at different redshifts. Hence, the number we find must be regarded as an upper limit.

If the radio emission detected in CIZAJ1938.3+5409 is due to the same mechanism that powers the halo for the $P_{1.4\,GHz}$–SZ correlation, the cluster should be undergoing a merger, one that has not left a strong imprint in the X-ray emission (see Section 4.1). We note that the cluster lies in a rather empty quadrant of the morphological diagram $c - w$ (Fig 11), in agreement with the hypothesis that we are observing it during a short phase in transition between merging and non-merging clusters.

The two possible scenarios described above make very different predictions: if we are observing a very rare object in its rapid transition between the radio-quiet and radio-loud phases, we expect to observe few objects of this type in large cluster samples. Instead, if the halo has a hadronic origin, radio emission will be detected in every massive cluster (the upper limits in Fig. 12). The detection of hadronic haloes would also allow us to constrain the energy budget in CR protons in the ICM.

Future deep radio surveys performed e.g. with LOFAR (van Haarlem et al. 2013) and later on with the Square Kilometre Array will shed light on this (Cassano et al. 2014).

5 CONCLUSIONS

In this work we have presented and analysed the radio emission from four galaxy clusters selected from the *Planck* catalogue (Planck Collaboration et al. 2011). The clusters are all massive, with $M_{500} > 6 \times 10^{14}\,M_\odot$, and are good candidates to host radio diffuse emission. We have used the same procedure to reduce and analyse the radio emission from the clusters and, with the help of *Chandra* archival data, we have performed a substructure analysis to quantify the dynamical status of the clusters. We have detected three radio haloes and we have placed one new upper limit in the $P_{1.4\,GHz}$–SZ plane.

Detection of diffuse radio sources in three out of four newly observed clusters, or in four out of five if we consider the previously published results on CL1821+643 (Bonafede et al. 2014) selected from the same SZ sample (Planck Collaboration et al. 2011), is indicative of a high fraction of occurrence of radio haloes in SZ selected samples. Such a high percentage has previously been suggested based on the analysis of NVSS radio images of *Planck* clusters (Sommer & Basu 2014). The small sample size of the current work does not permit us to make any statistical predictions. However, the first *Planck* catalogue (Planck Collaboration et al. 2011) shows no net bias with respect to the later *Planck* SZ catalogues (e.g. Planck Collaboration et al. 2013)] at high signal-to-noise ratio (corresponding to $M_{500} > 8 \times 10^{14}\,M_\odot$). Hence, any conclusion we may draw on the high radio halo fraction will be equally valid for later, more complete SZ catalogues.

Our results can be summarized as follows.

(i) We have discovered diffuse radio emission in three clusters, namely Abell 1443, CIZAJ1938.3+5409 and RXCJ0949.8+1708. In RXCJ0949.8+1708, a tentative radio halo was already claimed by Venturi et al. (2008).

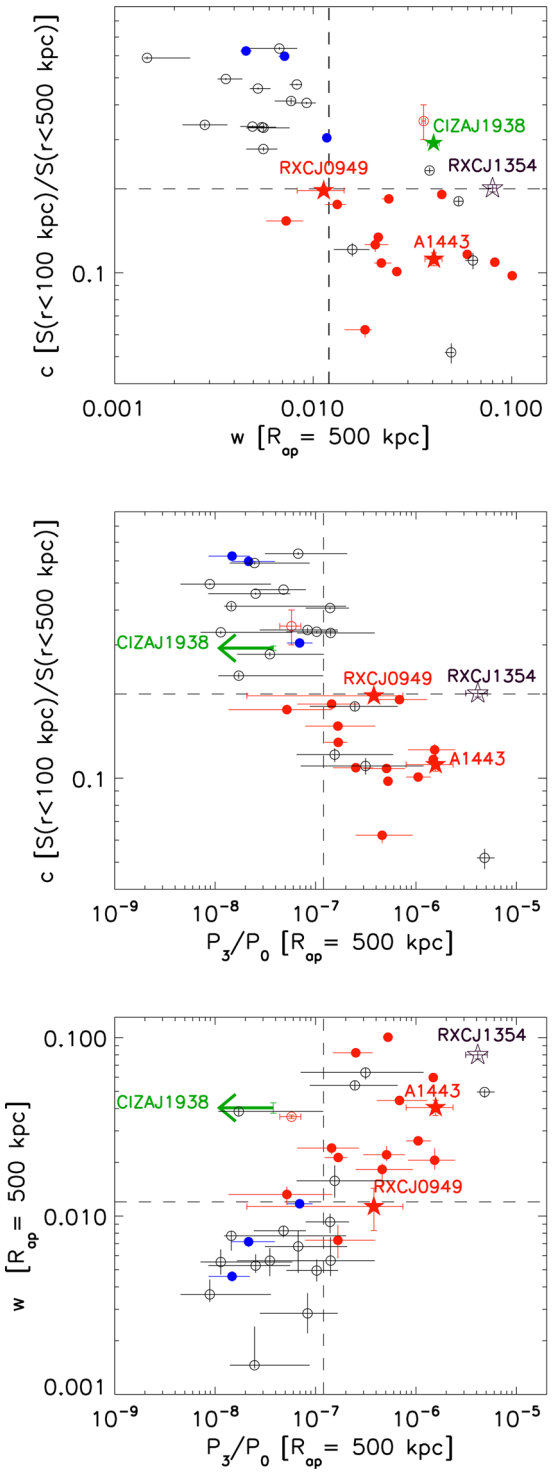

Figure 11. Morphological diagrams for $c - w$ (top), $c - P_3/P_0$ (middle) and $w - P - 3/P_0$, adapted from Cassano et al. (2010). Red filled symbols refer to radio haloes: red filled circles are from Cassano et al. (2010), the red empty circle is CL1821+643 from Bonafede et al (2014) and red filled stars are the radio haloes discovered in this article. Blue filled dots refer to to mini haloes, black circles are clusters with no radio emission (from Cassano et al. 2010). The green star and arrows refer to the low-power radio halo in CIZAJ1938.3+5409. Arrows are upper limits to the P_3/P_0 value. [A colour version is available in the on-line version.]

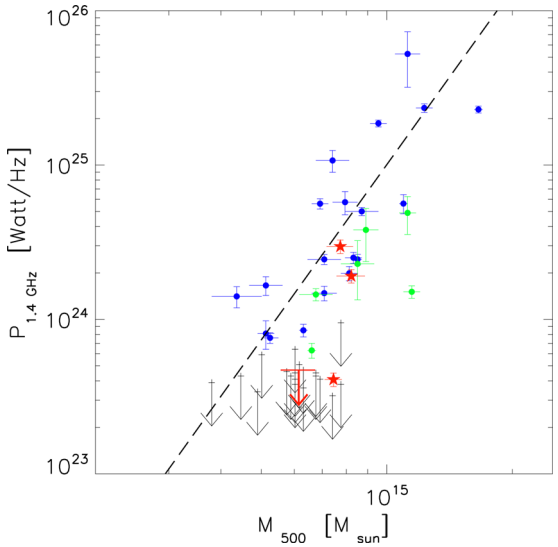

Figure 12. Correlation between the radio power of radio haloes at 1.4 GHz and the cluster mass M_{500} as derived by SZ measurements (Planck Collaboration et al. 2013). Blue points are the radio haloes used to derive the best-fitting line (shaded line). Green points are haloes with spectral index $\alpha > 1.5$. Arrows are upper limits (points, arrows and best-fitting lines taken from Cassano et al. 2013). Red filled stars are the radio haloes presented in this article, for which a spectral index $\alpha = 1.2$ is assumed. The red arrow refers to the upper limit on RXCJ1354.6+7715 (halo size ~700 kpc, $3\sigma_{\rm LR}$ detection threshold, see text for details). [A colour version is available in the on-line version.]

(ii) Clusters that fall in the same region of the morphological diagrams for P_3/P_0, w and c either can or cannot host a radio halo and their power either can or cannot follow the correlation, indicating that the dynamical status is not the only cause of radio emission.

(iii) The cluster Abell 1443 hosts peculiar emission, which does not obviously fall into the categories of radio halo or radio relic. A bright Γ-shaped source is found at the cluster centre, which we interpret as bright filamentary emission, similar to that found in MACSJ0717+3745 (Bonafede et al. 2009; van Weeren et al. 2009b). Alternatively, it could be a peculiar wide-angle tail radio galaxy.

(iv) The cluster CIZAJ1938.3+5409 hosts diffuse emission that we classify as a radio halo. The total power of the halo at 1.4 GHz, assuming a conservative $\alpha = 1.2$, would be a factor of eight below the $P_{1.4\,\rm GHz}$–SZ correlations, placing the cluster in the 'radio-quiet' zone. The cluster could be caught in its rapid (~0.1–0.2 Gyr) transition phase between the $P_{1.4\,\rm GHz}$–SZ correlation and the upper-limit region of the $P_{1.4\,\rm GHz}$–SZ plane, although no evident signs for an ongoing merger are visible in the X-ray image.
Alternatively, it could be the first direct detection of a hadronic radio halo. We have verified that this hypothesis is consistent with the most recent γ-ray upper limits by *Fermi* (Ackermann et al. 2014).

Information about the spectral index will be helpful to discriminate between the two possibilities or to point towards a different origin of the radio emission. It remains to be understood, however, whether this kind or low-power radio emission is common to all massive clusters or not. In any case, this is the first direct detection of a cluster in its radio-off state.

(v) The cluster RXCJ0949.8+1708 hosts diffuse emission on an Mpc scale that we classify as a radio halo. The emission is elongated

in the north–south direction and does not follow the X-ray emission from the gas. Although previous analysis based on optical and X-ray observations indicates that the cluster is not in a merging stage, the X-ray morphological estimators suggest that the cluster is borderline between merger and non-merger clusters.

(vi) No diffuse radio emission is detected in RXCJ1354.6+7715 at the sensitivity reached by our observations. Considering a halo size of ∼700 kpc and a detection threshold of $3\sigma_{\rm LR}$, we have placed an upper limit on the radio emission that is a factor of ∼5 below the $P_{1.4\,\rm GHz}$–SZ correlation.

ACKNOWLEDGEMENTS

The authors thank C. Jones for useful discussions. AB, MB, FV and FdG acknowledge support by the research group FOR 1254, funded by the Deutsche Forschungsgemeinschaft: 'Magnetisation of interstellar and intergalactic media: the prospects of low-frequency radio observations'. We thank the staff of the GMRT that made these observations possible. GMRT is run by the National Centre for Astrophysics of the Tata Institute of Fundamental Research. This research made use of the NASA/IPAC Extragalactic Data Base (NED), which is operated by the JPL, California Institute of Technology under contract with the National Aeronautics and Space Administration.

This publication makes use of data products from the Wide-field Infrared Survey Explorer, which is a joint project of the University of California, Los Angeles, and the Jet Propulsion Laboratory/California Institute of Technology, funded by the National Aeronautics and Space Administration.

REFERENCES

Ackermann M. et al., 2014, ApJ, 787, 18
Basu K., 2012, MNRAS, 421, L112
Blasi P., Colafrancesco S., 1999, Astroparticle Phys., 12, 169
Bock D. C.-J., Large M. I., Sadler E. M., 1999, AJ, 117, 1578
Böhringer H. et al., 2000, ApJS, 129, 435
Böhringer H. et al., 2010, A&A, 514, A32
Bonafede A. et al., 2009, A&A, 503, 707
Bonafede A., Feretti L., Murgia M., Govoni F., Giovannini G., Dallacasa D., Dolag K., Taylor G. B., 2010, A&A, 513, A30
Bonafede A., Govoni F., Feretti L., Murgia M., Giovannini G., Brüggen M., 2011a, A&A, 530, A24+
Bonafede A. et al., 2012, MNRAS, 426, 40
Bonafede A., Vazza F., Brüggen M., Murgia M., Govoni F., Feretti L., Giovannini G., Ogrean G., 2013, MNRAS, 433, 3208
Bonafede A. et al., 2014, MNRAS, 444, L44
Brown S., Emerick A., Rudnick L., Brunetti G., 2011, ApJ, 740, L28
Brunetti G., Jones T. W., 2014, Int. J. Modern Phys. D, 23, 1430007
Brunetti G., Lazarian A., 2011, MNRAS, 410, 127
Brunetti G., Setti G., Feretti L., Giovannini G., 2001, MNRAS, 320, 365
Brunetti G. et al., 2008, Nat, 455, 944
Brunetti G., Cassano R., Dolag K., Setti G., 2009, A&A, 507, 661
Buote D. A., 2001, ApJ, 553, L15
Buote D. A., Tsai J. C., 1995, ApJ, 452, 522
Cassano R., Ettori S., Giacintucci S., Brunetti G., Markevitch M., Venturi T., Gitti M., 2010, ApJ, 721, L82
Cassano R. et al., 2013, ApJ, 777, 141
Cassano R. et al., 2014. Cluster Radio Haloes at the Crossroads Between Astrophysics and Cosmology in the SKA Era. Giardini Naxos, Italy, p. 73
Condon J. J., Cotton W. D., Greisen E. W., Yin Q. F., Perley R. A., Taylor G. B., Broderick J. J., 1998, AJ, 115, 1693
Cotton W. D., 2008, PASP, 120, 439
Cuciti V., Cassano R., Brunetti G., Dallacasa D., Kale R., Ettori S., Venturi T., 2015, A&A, 580, A97
Dennison B., 1980, ApJ, 239, L93
Dolag K., Enßlin T. A., 2000, A&A, 362, 151
Donnert J., Dolag K., Cassano R., Brunetti G., 2010, MNRAS, 407, 1565
Donnert J., Dolag K., Brunetti G., Cassano R., 2013, MNRAS, 429, 3564
Ebeling H., Edge A. C., Allen S. W., Crawford C. S., Fabian A. C., Huchra J. P., 2000, MNRAS, 318, 333
Ebeling H., Mullis C. R., Tully R. B., 2002, ApJ, 580, 774
Ebeling H., Edge A. C., Mantz A., Barrett E., Henry J. P., Ma C. J., van Speybroeck L., 2010, MNRAS, 407, 83
Enßlin T., Pfrommer C., Miniati F., Subramanian K., 2011, A&A, 527, A99
Feretti L., Giovannini G., Govoni F., Murgia M., 2012, A&AR, 20, 54
Giocoli C., Moreno J., Sheth R. K., Tormen G., 2007, MNRAS, 376, 977
Giovannini G., Tordi M., Feretti L., 1999, New Astron., 4, 141
Giovannini G., Feretti L., Girardi M., Govoni F., Murgia M., Vacca V., Bagchi J., 2011, A&A, 530, L5
Govoni F. et al., 2010, A&A, 522, A105+
Horesh A., Maoz D., Ebeling H., Seidel G., Bartelmann M., 2010, MNRAS, 406, 1318
Intema H. T., van der Tol S., Cotton W. D., Cohen A. S., van Bemmel I. M., Röttgering H. J. A., 2009, A&A, 501, 1185
Intema H. T., van Weeren R. J., Röttgering H. J. A., Lal D. V., 2011, A&A, 535, A38
Kale R. et al., 2015, A&A, 579, A92
Kelner S. R., Aharonian F. A., Bugayov V. V., 2006, Phys. Rev. D, 74, 034018
Kushnir D., Katz B., Waxman E., 2009, J. Cosmol. Astropart. Phys., 09, 024
Khatri R., 2015, preprint (arXiv:1505.00778)
Lane W. M., Cotton W. D., van Velzen S., Clarke T. E., Kassim N. E., Helmboldt J. F., Lazio T. J. W., Cohen A. S., 2014, MNRAS, 440, 327
Liang H., Hunstead R. W., Birkinshaw M., Andreani P., 2000, ApJ, 544, 686
Maughan B. J., Jones C., Forman W., Van Speybroeck L., 2008, ApJS, 174, 117
Petrosian V., 2001, ApJ, 557, 560
Pfrommer C., Enßlin T. A., 2004a, A&A, 413, 17
Pfrommer C., Enßlin T. A., 2004b, A&A, 426, 777
Planck Collaboration et al., 2011, A&A, 536, A8
Rengelink R. B., Tang Y., de Bruyn A. G., Miley G. K., Bremer M. N., Roettgering H. J. A., Bremer M. A. R., 1997, A&AS, 124, 259
Santos J. S., Rosati P., Tozzi P., Böhringer H., Ettori S., Bignamini A., 2008, A&A, 483, 35
Scaife A. M. M., Heald G. H., 2012, MNRAS, 423, L30
Sommer M. W., Basu K., 2014, MNRAS, 437, 2163
van Haarlem M. P. et al., 2013, A&A, 556, A2
van Weeren R. J., Röttgering H. J. A., Brüggen M., Cohen A., 2009b, A&A, 505, 991
van Weeren R. J. et al., 2012, A&A, 543, A43
Vazza F., Eckert D., Brueggen M., Huber B., 2015, A&A, 580, A119
Venturi T., Giacintucci S., Dallacasa D., Cassano R., Brunetti G., Bardelli S., Setti G., 2008, A&A, 484, 327
Wright E. L. et al., 2010, AJ, 140, 1868
Zandanel F., Pfrommer C., Prada F., 2014, MNRAS, 438, 124

This paper has been typeset from a TEX/LATEX file prepared by the author.